AFRL-ML-WP-TP-2006-440

SPATIAL CORRELATION COEFFICIENT IMAGES FOR ULTRASONIC DETECTION (PREPRINT)

Raina Cepel, K.C. Ho, Brett A. Rinker, Donald D. Palmer, Jr., Terrence P. Lerch, and Steven P. Neal

JULY 2006

Approved for public release; distribution is unlimited.

STINFO COPY

MATERIALS AND MANUFACTURING DIRECTORATE
AIR FORCE RESEARCH LABORATORY
AIR FORCE MATERIEL COMMAND
WRIGHT-PATTERSON AIR FORCE BASE, OH 45433-7750

REPORT DOCUMENTATION PAGE

Form Approved
OMB No. 0704-0188

1. REPORT DATE *(DD-MM-YY)*	2. REPORT TYPE	3. DATES COVERED *(From - To)*
July 2006	Journal Article Preprint	01/01/2005 – 12/31/2005

4. TITLE AND SUBTITLE
SPATIAL CORRELATION COEFFICIENT IMAGES FOR ULTRASONIC DETECTION (PREPRINT)

5a. CONTRACT NUMBER
FA8650-04-C-5704

5b. GRANT NUMBER

5c. PROGRAM ELEMENT NUMBER
62102F

6. AUTHOR(S)
Raina Cepel and Steven P. Neal (University of Missouri-Columbia/Mechanical and Aerospace Engineering)
K.C. Ho (University of Missouri-Columbia/Electrical and Computer Engineering)
Brett A. Rinker (Honeywell Federal Manufacturing and Technology)
Donald D. Palmer, Jr. (The Boeing Company)
Terrence P. Lerch (Central Michigan University)

5d. PROJECT NUMBER
2510

5e. TASK NUMBER
00

5f. WORK UNIT NUMBER
00

7. PERFORMING ORGANIZATION NAME(S) AND ADDRESS(ES)

University of Missouri-Columbia
Mechanical and Aerospace Engineering
E3401 Lafferre Hall
Columbia, MO 65211

University of Missouri-Columbia
Electrical and Computer Engineering
Columbia, MO 65211

Honeywell Federal Manufacturing and Technology
Kansas City, MO

The Boeing Company, Phantom Works
St. Louis, MO

Central Michigan University
Engineering and Technology
Mount Pleasant, MI 48859

8. PERFORMING ORGANIZATION REPORT NUMBER

9. SPONSORING/MONITORING AGENCY NAME(S) AND ADDRESS(ES)
Materials and Manufacturing Directorate
Air Force Research Laboratory
Air Force Materiel Command
Wright-Patterson AFB, OH 45433-7750

10. SPONSORING/MONITORING AGENCY ACRONYM(S)
AFRL-ML-WP

11. SPONSORING/MONITORING AGENCY REPORT NUMBER(S)
AFRL-ML-WP-TP-2006-440

12. DISTRIBUTION/AVAILABILITY STATEMENT
Approved for public release; distribution is unlimited.

13. SUPPLEMENTARY NOTES
This work, resulting in whole or in part from Department of the Air Force contract FA8650-04-C-5704, has been submitted to IEEE for publication in the IEEE Transactions on Ultrasonics, Ferroelectrics, and Frequency Control. If this work is published, IEEE may assert copyright. The United States has for itself and others acting on its behalf an unlimited, paid-up, nonexclusive, irrevocable worldwide license to use, modify, reproduce, release, perform, display, or disclose the work by or on behalf of the Government. All other rights are reserved by the copyright owner. PAO Case Number: AFRL/WS 06-1706, 10 Jul 2006.

14. ABSTRACT
In ultrasonics, image formation and detection are generally based on signal amplitude. In this paper, we describe an amplitude independent approach for image formation and detection based on the similarity of adjacent signals. Signal similarity is quantified in terms of the correlation coefficient calculated between A-scans digitized at adjacent measurement positions. Correlation coefficient images are introduced for visualizing the similarity in measured A-scans. In backscatter, the approach reveals defect signals buried in noise by showing regions of increased correlation. In pitch-catch or thru-transmission, the approach reveals defects by showing regions of decreased correlation due to signal distortion caused by interaction of the beam field with the defect. Correlation coefficient and C-scan images are shown to demonstrate flat-bottom-hole detection in a stainless steel annular ring and crack detection in an aluminum aircraft structure. Simulated data are used to show the detection of planar defects at very low signal-to-noise ratio.

15. SUBJECT TERMS ultrasonics, acoustic noise, spatial correlation, aging aircraft, nondestructive inspection

16. SECURITY CLASSIFICATION OF:			17. LIMITATION OF ABSTRACT:	18. NUMBER OF PAGES	19a. NAME OF RESPONSIBLE PERSON (Monitor)
a. REPORT	b. ABSTRACT	c. THIS PAGE			Gary Steffes
Unclassified	Unclassified	Unclassified	SAR	28	19b. TELEPHONE NUMBER *(Include Area Code)* N/A

Standard Form 298 (Rev. 8-98)
Prescribed by ANSI Std. Z39-18

Spatial correlation coefficient images for ultrasonic detection

Raina Cepel,[1] K. C. Ho, [2] Brett A. Rinker, [3] Donald D. Palmer, Jr., [4] Terrence P. Lerch, [5] and Steven P. Neal[1]

[1] Mechanical and Aerospace Engineering
[2] Electrical and Computer Engineering
University of Missouri-Columbia, Columbia, MO 65211

[3] Honeywell Federal Manufacturing and Technology, Kansas City, MO
[4] The Boeing Company, Phantom Works, St. Louis, MO
[5] Engineering and Technology, Central Michigan University,
Mount Pleasant, MI 48859

Brief title: Correlation coefficient images

Abstract:

In ultrasonics, image formation and detection are generally based on signal amplitude. In this paper, we describe an amplitude independent approach for image formation and detection based on the similarity of adjacent signals. Signal similarity is quantified in terms of the correlation coefficient calculated between A-scans digitized at adjacent measurement positions. Correlation coefficient images are introduced for visualizing the similarity in measured A-scans. In backscatter, the approach reveals defect signals buried in noise by showing regions of increased correlation. In pitch-catch or thru-transmission, the approach reveals defects by showing regions of decreased correlation due to signal distortion caused by interaction of the beam field with the defect. Correlation coefficient and C-scan images are shown to demonstrate flat-bottom-hole detection in a stainless steel annular ring and crack detection in an aluminum aircraft structure. Simulated data are used to show the detection of planar defects at very low signal-to-noise ratio.

PACS numbers: 43.20.Hq, 43.20.Ye, 43.20.-f, 43.35.Cg

I. Introduction

Typical ultrasonic detection in nondestructive evaluation (NDE) is amplitude based. In the simplest case, an echo signal above a threshold or a transmitted signal below a threshold form the basis for detection. C-scan images are used to display peak-amplitudes throughout a scan. Based on a C-scan image, regions of high or low amplitude can be identified either manually or using a computer decision based approach. A weakness of amplitude based approaches is their direct and inherent sensitivity to non-defect related amplitude changes associated with the measurement system or sample. In this paper, we focus on a complimentary detection approach which relies on the correlations between adjacent A-scans as a basis for detection.[1-3] Correlation coefficient images are introduced for visualizing the similarity in measured A-scans. Rather than using signal amplitude, this approach bases detection on the similarity, or lack of similarity, between adjacent signals. In backscatter, this approach reveals defect signals buried in noise by showing regions of increased correlation. In pitch-catch or thru-transmission, the approach reveals defects by showing regions of decreased correlation due to signal distortion caused by interaction of the beam field with the defect.

The basic approach for forming correlation images as described in this paper uses the same A-scans which form the basis of C-scan images. In either case, the process begins with measured A-scans written into a three-dimensional matrix with the rows and columns of the matrix registered with the measurement locations and with the A-scans written into the third dimension (see Fig. 1). A C-scan image is typically formed by establishing a time gate, finding the maximum absolute value (or maximum min-to-max deviation) within the time gate for each A-scan, writing these maximum values into a two-dimensional matrix which mimics the scan pattern, and forming an image based on this two-dimensional matrix. Formation of a correlation

image is more complicated, but the basic approach is the same: establish a time gate, calculate the correlation coefficient between adjacent A-scan in the three-dimensional matrix, write these correlations into a two-dimensional matrix, and form a correlation image based on these correlations. As will be discussed, complications arise from: initial alignment of A-scans, local alignment of signals, skipping signal measurement positions, and image formation using matrices with blank elements.

The correlation approach addressed here contains at least an element of matched filtering. Matched filtering is a technique commonly used in radar to optimize the signal to noise ratio (SNR). Matched filter theory states that when choosing a finite impulse response filter to optimize SNR of a received signal, the ideal filter will have the same frequency content as the defect signal to be detected. The application of matched filtering in radar, optics and acoustics has an extensive history, whether applied classically (see, e.g., references 4-11) or adaptively (see, e.g., references 12-17). However, challenges still remain relative to *a priori* determination of the frequency content of unknown, and yet to be detected, defect signals. As applied to defect detection using ultrasonics, implementation of the matched filter is comparable to cross-correlating the expected defect signal (the "template") with each received A-scans and using high correlation values as a basis for detection. The efficacy of this technique as applied to ultrasonics is directly related to the quality of the template, that is, the filter's efficacy is related to the operator's ability to establish of the frequency content of the defect signal to be detected. Accounting for the influence of scattering by an unknown defect on the frequency content of the defect signal is particularly difficult. In the correlation approach presented in this paper, each signal is correlated with its nearest neighbors. In essence, each gated A-scan is taken to be a template for application of matched filtering to gated A-scans measured at neighboring

measurement positions, with high correlations again used as a basis for detection. To some degree, the neural processes of a human observer are being mimicked by the correlation approach. For example, an observer of a B-scan image will notice local similarities in A-scans making up the B-scan – even if distorted in unpredictable or unknown ways, the observer will detect the similarity.

The remainder of this paper deals with the details of the correlation approach. The paper begins by addressing the procedures used in measuring A-scans and for creating simulated A-scans. Correlation calculations and issues associated with signal alignment and correlation image display are then addressed. Correlation images are presented in the results section based on the measured and simulated A-scans. C-scan images are also presented for comparison purposes with the new correlation images. The paper closes with a summary and discussion section.

II. Measured and simulated A-scans

A-scans were measured in an immersion mode from three samples: a stainless steel plate; a stainless steel annular ring with nominal inside and outside diameters of 40 mm and 70 mm, respectively; and an aluminum sample fabricated to represent an aircraft structure. A Panametrics 10 MHz, ½" diameter, 4" focal length transducer was used in scanning the plate sample at normal incidence on a 45 x 62 regular grid with 0.5 mm between measurement positions. Data from the plate sample was used to show grain noise correlation images at different measurement position spacing and as a basis for creating simulated noise signals. The annular ring sample was machined to add five equal-depth flat bottom holes. A Panametrics 15 MHz, ½" diameter, 6" focal length transducer was used for a polar scan at normal incidence on the annual sample with 2 degrees between radial scan lines and 0.762 mm between

circumferential scan lines. Data from the annular sample was used to show polar correlation images and to present correlation images for flat-bottom-hole signals within grain noise. The aluminum sample was comprised of two aluminum plates fastened together with EDM notches of various lengths extending from selected fastener holes. For the aluminum sample, oblique incident pitch-catch measurements were made using a pair of Panametrics 10 MHz, ½" diameter, transducers, one flat and one with a focal length of 3". Transducers were arranged 5 degrees from normal. The aluminum sample with simulated cracks was used to demonstrate the use of correlation images for the detection of cracks based on lack of correlation in transmitted signals.

A-scans were also created using simulated defect signals buried within simulated grain noise. Gaussian damped sinusoids were used to simulate defect signals with the appropriate frequency content. To simulate planar defects with varying aspect ratio and at various signal-to-noise ratios, defect signals were scaled over certain spatial regions and added to the simulated noise signals. This process is represented in equation form for a signal measured at the *ij* position in a simulated raster scan as follows:

$$x(i,j,t) = n(i,j,t) + B(i,j)y(t) \tag{1}$$

where $n(i,j,t)$ represents simulated acoustic noise before the addition of a defect signal, $y(t)$, scaled by $B(i,j)$, a scale factor which can be varied over lateral space, and $x(i,j,t)$ is the result, representing the simulated measurement data. The computation is carried out over all noise signals. Simulated grain noise signals were generated to mimic the maximum extreme value (gated peak value) distribution and correlation coefficient distribution associated with the measured noise from the stainless steel plate sample.[18] The basic procedure involves creating

each simulated A-scan as a scaled version of previously generated signals plus a new random noise component. Desired correlation values between signals are drawn at random from correlation coefficient distributions established using the measured noise. The maximum extreme value distribution associated with the simulated signals is controlled through the standard deviation of the random number generator, by scaling the signals to control signal energy, and by filtering the signals to yield the same frequency content as the measured signals. The details of this procedure are beyond the scope of this paper, but will be documented elsewhere.

III. Formation of correlation images

A. Basic correlation coefficient calculation

The correlation of interest is the spatial cross-correlation calculated between gated A-scans measured at adjacent measurement positions. Consider an *N x M* scan with each A-scan *T* points long and using the matrix $\mathbf{x} = x(i,j,t) \quad i = 1...N \quad j = 1...M \quad t = 0...T-1$ to hold the A-scans (see Fig. 1). Calculation of the correlation coefficient between A-scans is then given by the following equation where $\hat{\rho} = \hat{\rho}(i,j,\delta_r,\delta_c,\tau)$ is a sample estimate of the associated expected value:[19]

$$\hat{\rho} = \frac{\sum_{t=t_i}^{t_f} [x(i,j,t-\tau) - m_x(i,j)][x(i+\delta_c, j+\delta_r, t) - m_x(i+\delta_c, j+\delta_r)]}{\sqrt{\sum_{t=t_i}^{t_f} [x(i,j,t-\tau) - m_x(i,j)]^2} \sqrt{\sum_{t=t_i}^{t_f} [x(i+\delta_c, j+\delta_r, t) - m_x(i+\delta_c, j+\delta_r)]^2}} \qquad (2)$$

Normalization removes the scale dependence and restricts $\hat{\rho}$ to the range -1 to 1. In Eq. (2), the summation range in the time-domain defines the portion of the signal (the time window or gate) of interest, m_x and m_y are mean values calculated over the gate, τ controls the lag or temporal shift between the two signals, and δ is a spatial shift parameter. Throughout the paper, t is used as a discrete index referring to the temporal direction. With $\delta_r = 1,\ \delta_c = 0$, row correlation are calculated between adjacent A-scan, that is, A-scans measured at the j^{th} and $j^{th}+1$ positions in the i^{th} scan row. Similarly, with $\delta_r = 0,\ \delta_c = 1$, column correlations can be calculated. Correlations for all possible adjacent signal combinations in an *N x M* raster scan can be established using a computation loop over *i* and *j* with the spatial shift applied sequentially to *i* and *j*. Correlations can also be calculated with signals systematically skipped by setting the spatial shift parameters to an integer greater than one, for example, with $\delta_r = 2\ \delta_c = 0$, row correlations are calculated for every other signal.

B. Signal alignment

As a point of motivation, consider the same material solid-state welding problem where the front surface of the part is nominally flat and parallel to the weld plane.[20,21] Signal misalignment can result from errors in the mechanical scan, systematic or random variations in the front surface, and systematic or random weld-surface irregularities. As such, signal alignment will be addressed in terms of global alignment using front surface reflections and then local alignment based on gated A-scans.

Global signal alignment for backscatter is done by aligning the leading edge of each front surface reflection. In general, when interrogating the volume of a component for defects, the front surface reflection is blown off scale, making most of the front surface reflection truncated

and difficult to use in a signal processing sense. Nevertheless, the signals can be aligned based on the front surface reflection leading edge by applying any number of signal processing approaches, including alignment of trigger points as used here. Global alignment yields B-scan images aligned at the front surface reflection, providing a basis for evaluating the remaining systematic or random misalignment in the weld plane signal. This global alignment is only achieved easily and unambiguously under certain measurement configurations and sample geometries.

Local signal alignment can be used to form locally aligned B-scan images or to form correlation coefficient images based on maximum correlations. In either case, the core process involves forming a cross-correlelogram between two signals. The cross-correlelogram, which looks at the correlation between signals as one signal is shifted in time relative to the other signal, is given by a plot of $\hat{\rho}(\tau)$ versus τ. From this plot, the maximum correlation and the shift to the maximum correlation can be extracted.

To perform local signal alignment for B-scan images, each gated signal is aligned to a single signal which has been chosen as the reference alignment signal. Any signal in a scan could be used as the reference signal; however, we typically choose the signal that has the greatest voltage within the time gate. Alignment is achieved based on the time-shift to the maximum correlation between each signal and the reference signal as discussed above. Again, consider same material solid state welding between two polycrystalline metals. If the weld is inadequate resulting in an echo signal from the weld plane, the alignment procedure will align the weld plan signals and yield B-scan images with a relatively smooth stripe at the time corresponding to the weld plane position. Conversely, a perfect weld will yield only

backscattered grain noise, and the alignment procedure will result in B-scans which show at most short stripes randomly distributed in time.

To perform local signal alignment to be used in correlation images, we calculate the cross-correlelogram between each gated signal and its nearest row and column neighbors. The maximum correlation value is then extracted from the plot of $\hat{\rho}(\tau)$ versus τ for each pair of signals. For an *N x M* scan where correlations are calculated with no signals skipped, there will be $N(M-1)$ row correlations and $(N-1)M$ column correlations, for a total number of $2NM-M-N$ correlations which will be used as a basis for forming the correlation image. Figure 2 shows a schematic representation of a 4 x 4 scan (left figure) with open circles at the 16 measurement positions. The R's and C's are used to represent the positions conceptually assigned to the correlation between adjacent row signals and adjacent column signals, respectively. Also shown in the figure is a portion of a polar scan (right figure) with the R's and C's now representing the positions assigned to radial and circumferential correlations, respectively, and the open circles again at the measurement positions.

C. Image display issues

Whether before or after signal alignment, there are issues associated with displaying the $N(M-1)+(N-1)M$ correlation values as an image. For discussion purposes, again consider a 4 x 4 raster scan. Nearest neighbor correlations will result in a 4 x 3 set of row correlations and a 3 x 4 set of column correlations as is apparent from Fig. 2. At this point, the easiest approach would be to make two correlation images: one for the row correlations and one for the column correlations. Similarly, radial and circumferential correlation images could be made for a polar scan. This procedure yields two correlation images which allow separate evaluation of row and column correlations.

The issues associated with forming a single correlation image can be addressed by first thinking in terms of writing the row and column correlations into a single matrix. For the 4 x 4 example, to maintain spatial registration, the 4 x 3 row correlations and the 3 x 4 column correlations would be written into a 7 x 7 matrix (see Fig. 2). For this example, the difficulty is that only 24 correlation coefficients are written into a 49 position matrix, leaving 25 blank elements. These blank elements spatially correspond to the measurement positions (open circles in Fig. 2) and to the centroid of the region defined by each set of four measurement positions (solid circles in Fig. 2). In general terms, the $N(M-1)+(N-1)M$ row and column correlations are written into a $(2N-1)\,x\,(2M-1)$ matrix, leaving $2NM-N-M+1$ blank elements. An image based directly on a matrix with blank elements, with each blank element assigned the same value, is visually unsatisfying with useful correlation values displayed within a regular array of mono-colored pixels.

A variety of solutions exist to this image display problem. One potential solution would be to assign each blank element an average of nearest neighbor values. The resultant image would be composed of pixels associated with row correlations and column correlations and pixels which are an average of row and column correlations. A second approach is to shift the column correlations up one row. This approach compromises spatial registration; however, as shown in the results section, the resultant images are useful for qualitative evaluation. A third approach which preserves spatial registration is to consider each correlation value as being centered in a diamond-shape region. This approach can be applied to both Cartesian and polar scan data as depicted in Fig. 2. For the 4 x 4 example, the image would have 4 rows of 3 diamonds (row correlations) interleaved with 3 rows of 4 diamonds (column correlations). To facilitate display of these diamond regions, a matrix with a much higher number of elements than

the original correlation matrix is used to approximate the diamond-shaped regions, that is, the diamonds are discretized (see Fig. 3). Each element in the high density matrix is assigned a value based on which diamond that element falls within. The pixels outside of the diamond-filled regions are set to a single (arbitrary) value. As shown in the blown-up polar correlation images in Fig. 4, a close look at each diamond region in a correlation image reveals this discretization with each diagonal line having a saw-toothed appearance at the scale of the high density matrix and the outside edges of the image having a saw-toothed appearance at the scale of the diamond regions.

IV. Results

Example results were chosen to cover measured and simulated data, *xy* and polar scans, planar and localized defects, and detection based on increased and decreased correlation, respectively. In each case, companion C-scan images are shown for comparison purposes.

Figure 5 shows a correlation image (top) and C-scan image (bottom) for the stainless steel annular ring. Data were measured in a polar scan with the correlation image displayed using the diamond region format. The regions of higher correlation and higher amplitude near the inside and outside diameter are due to multiple reflected signals from surfaces not in the plane of the flat-bottom-holes. The flat-bottom-hole diameters starting with the top hole and moving clockwise are 1/16", 2/16", 3/16", 3/16", and 3/16". In both images, the five flat-bottom-holes are clearly visible. Detection in the correlation images is possible due to increased correlation between signals containing echo signals from a given flat-bottom-hole.

Figure 6 shows three images based on simulated data generated as described above. The top figure is an image of the scale factor $B(i, j)$. This image represents a SNR mask which reveals the location and SNR of each of the simulated planar defects which were superimposed

on simulated acoustic noise. SNR is defined here as the ratio of the maximum extreme value of the signal to be added to the noise and the expected maximum extreme value of the noise. The SNR for each defect is indicated in the figure caption. Notice that the highest SNR is less than one. The middle image in Fig. 6 is a C-scan image. Even at the very low SNR's, given the lateral extent of the defects, three out of five defects are visible in the C-scan image. A fourth defect also visible, especially given the bias created by knowing the defect locations. The lower image is a correlation image formed using the interleaving approach. In this image, four of the defects are easily detected with the region around the fifth defect also arguably of concern.

The final example is based on measured oblique incidence pitch-catch data from the aluminum sample. The schematic in Fig. 7 shows the sample geometry. The sample is made up of two aluminum plates joined together with two rows of eight fasteners with sealant between the two plates. EDM slots were machined to extend from four of the fastener holes in the outer aluminum plate (the skin) at four different lengths as shown in the figure. Images are based on the back surface reflection (signal C) from the lower plate (the substructure). Similar results are obtained by monitoring signal B from the interface (the faying layer). In this case, interaction of the acoustic beam with the EDM slots causes amplitude reduction and distortion of the transmitted signal. The reduction in amplitude makes the presence of the cracks apparent in the C-scan image. The distortion leads to a reduction in signal correlation, making the cracks detectable in the correlation image. The three longer slots are easily detected and sized in either image with the 1 mm crack difficult to detect without optimized measurements and additional processing.

V. Summary and discussion

The correlation approach for defect detection outlined in this paper is attractive as a potential compliment to the classical C-scan approach for a number of reasons including: the correlation approach is scale independent; the correlation approach relies on signal shape, while the C-scan approach uses only the peak value; correlation images are calculated based on the same A-scans used in forming C-scan images; correlation images have a qualitatively similar appearance to C-scan images, which facilitates inspector acceptance; and at very low SNR, the correlation approach shows the potential to outperform the C-scan approach for detecting defects that show some lateral extent.

In terms of additional development on the correlation approach, work is underway on a number of fronts. A formal ROC analysis, which is underway, should shed light on the performance of the correlation approach alone and in combination with the C-scan approach relative to the performance of the C-scan approach alone. A matched filter approach will also be included in the analysis. The correlation approach is amplitude independent but is not measurement system and material independent. Preliminary assessment has shown very weak dependence of correlation values on the beam field near the focal region of a circularly focused piston-source transducer. Future work will include a more in depth study of the influence of beam field variations, frequency content, and material morphology on the correlation approach. Initial work has also been done in the area of statistical detection applied to the correlation approach with the goal of creating threshold images based on a specified false-call rate. We conclude by noting that this is only a partial list of issues to be considered in developing and evaluating this correlation-based approach to image formation and defect detection.

Acknowledgements

This work was supported by the Center for Aerospace Manufacturing Technology (CAMT) at the University of Missouri-Rolla funded under Air Force Research Laboratory Contract FA8650-04-C-5704 and by Boeing under PO Z40791. Previous support for development of the correlation approach was provided by Honeywell Federal Manufacturing and Technology and by the National Science Foundation (NSF CMS 9610189). The authors would like to acknowledge early development work on correlation analysis by Dr. Mark D. Russell while a postdoc at the University of Missouri-Columbia (MU). Thanks are also due Dr. Lori Thombs from the Department of Statistics at MU for her consultation on the project. The authors would also like to acknowledge the tremendous support from personnel at Honeywell FM&T including Eric Jamieson, Jose A. Samayoa, and Jason P. Miller. In particular, the encouragement by Eric Jamieson to extent the correlation approach to localized flaw detection was pivotal. Many thanks are also due to Dr. Zoughi from the University of Missouri-Rolla (UMR) for his technical guidance and leadership.

References

1. W. F. Walker, "The significance of correlation in ultrasound signal processing", *Proc. SPIE Vol. 4325, Medical Imaging: Ultrasonic Imaging and Signal Processing*, edited by Michael F. Insana and K. Kirk Shung, 2001, pp. 159-171.
2. A. Dogandzic and N. Eua-Anant, "Defect detection in correlated noise", *Review of Progress in Quantitative Nondestructive Evaluation*, Vol. 23A, edited by D. E. Chimenti and D. O. Thompson, AIP, Melville, 2004, pp. 628-635.
3. R. B. Thompson, L. Yu, and F. J. Margetan, "A formal theory for the spatial correlation of backscattered ultrasonic grain noise", *Review of Progress in Quantitative Nondestructive Evaluation*, Vol. 24, edited by D. E. Chimenti and D. O. Thompson, AIP, Melville, 2005, pp. 1292-1299.
4. D. R. Arsenault, P. Das, and L. B. Milstein, "Matched filtering of continuous signals by the product of transforms technique using SAW chip filters", *Ultrasonic Symposium*, 543-548, (1978).
5. R. J. Marks, II, L. E. Atas, J. J. Choi, s. Oh, K. F. Cheung, and D. C. Park, "Performance analysis of associative memories with nonlinearities in the correlation domain", *Appl. Opt.* **27**, 2900, (1988).

6. K. d. Konohue, J. M. Bressler, T. Varghese, and N. M. Bilgutay, "Spectral correlation in ultrasonic pulse echo signal processing", *IEEE Trans. Ultrason. Ferroelectr. Freq. Control*, **40**(4), 330-337, (1992).
7. H. Eriksson, P. O. Borjesson, P. Odling, and N. G. Holmer, "A robust correlation receiver for distance estimation", *IEEE Trans. Ultrason. Ferroelectr. Freq. Control*, **41**(5), 506-603, (1994).
8. A. Abbate, J. Koay, J. Frankel, S. C. Schroeder, and P. Das, "Signal detection and noise suppression using wavelet transform signal processor: application to ultrasonic flaw detection", *IEEE Trans. Ultrason. Ferroelectr. Freq. Control*, **44**(1), 13-26, (1997).
9. J. M. Seixas, F. P. Freeland, and W. Soares-Filho, "Matched filters for identifying failed fuel rods in nuclear reactors", Electronics, Circuits and Systems, 2001, ICECS 2001, The 8th IEEE International Conference on, 2, 643-646, (2001).
10. A. W. Meyer and J. V. Candy, "Iterative processing of ultrasonic measurements to characterize flaws in critical optical components", *IEEE Trans. Ultrason. Ferroelectr. Freq. Control*, **49(8)**, 1124-1138, (2002).
11. E. Biagi, N. Dreoni, L. Masotti, I. Rossi, and M. Scabia, "ICARUS: imaging pulse compression algorithm through remapping of ultrasound", *IEEE Trans. Ultrason. Ferroelectr. Freq. Control*, **52**(2), 261-279, (2005).
12. J. P. Hermand and W. I. Roderick, "Channel-adaptive matched fitler processing of large time-bandwidth signals: Preliminary results", JASA, **89**(4B), 2001, (1991).
13. K. A. Melendez and J. W. Modestino, "Spatiotemporal multiscan adaptive matched filtering", Proc. SPIE Vol 2561, Signal and Data Processign of Small Targets 1995, Oliver E Drummond, Editor, September 1995, 51-65, (1995).
14. D. O. Walsh, A. F. Gmitro, and M. W. Marcellin, "Adaptive reconstruction of phased array MR imagery", *Magnetic Resonance in Medicine*, **43**(5), 682-690, (2000).
15. S. Yon, M. Tanter, and M. Fink, "Sound focusing in rooms. II. The spatio-temporal inverse filter", JASA, 114(6), 3044-3052, (2003).
16. S. D. Blunt and K. Gerlach, "Efficient robust AMF using FRACTA algorithm, *IEEE Transactions on Aerospace and Electronic Systems*, **41**(2), 537-548, (2005).
17. M. C. Wicks, M. Rangaswamy, R. adve, and T. B. Hale, "Space-time adative processing", IEEE Signal Processing Magazine, **23**(1), 51-65, (2006).
18. F. J. Margetan, E. Nieters, L. Brasche, L. Yu, A. Degtyar, H. Wasan, M. Keller, and A. Kinney, "Fundamental Studies of Titanium Forging Materials - Engine Titanium Consortium II", FAA William J. Hughes Technical Center, Atlantic City, N. J., Report number DOT/FAA/AR-05/22 (June 2005).
19. J. S. Bendat and A. G. Piersol, *Engineering Applications of Correlation and Spectral Analysis*, J. Wiley, New York, p. 46, 1993.
20. P. B. Nagy and L. Adler, "Ultrasonic NDE of Solid State Bonds: Inertia and Friction Welds", *J. Nondestructive Eval*. **7(3/4)**, 199-215, (1988).
21. B. A. Rinker, E. E. Jamieson, J. A. Samayoa, T. G. Abeln, T. P. Lerch, and S. P. Neal, "Detection of weak interface signals for same material bond/weld inspection", *Review of Progress in Quantitative Nondestructive Evaluation*, Vol. 22B, edited by D. E. Chimenti and D. O. Thompson, AIP, Melville, 2003, pp. 1080-1087.

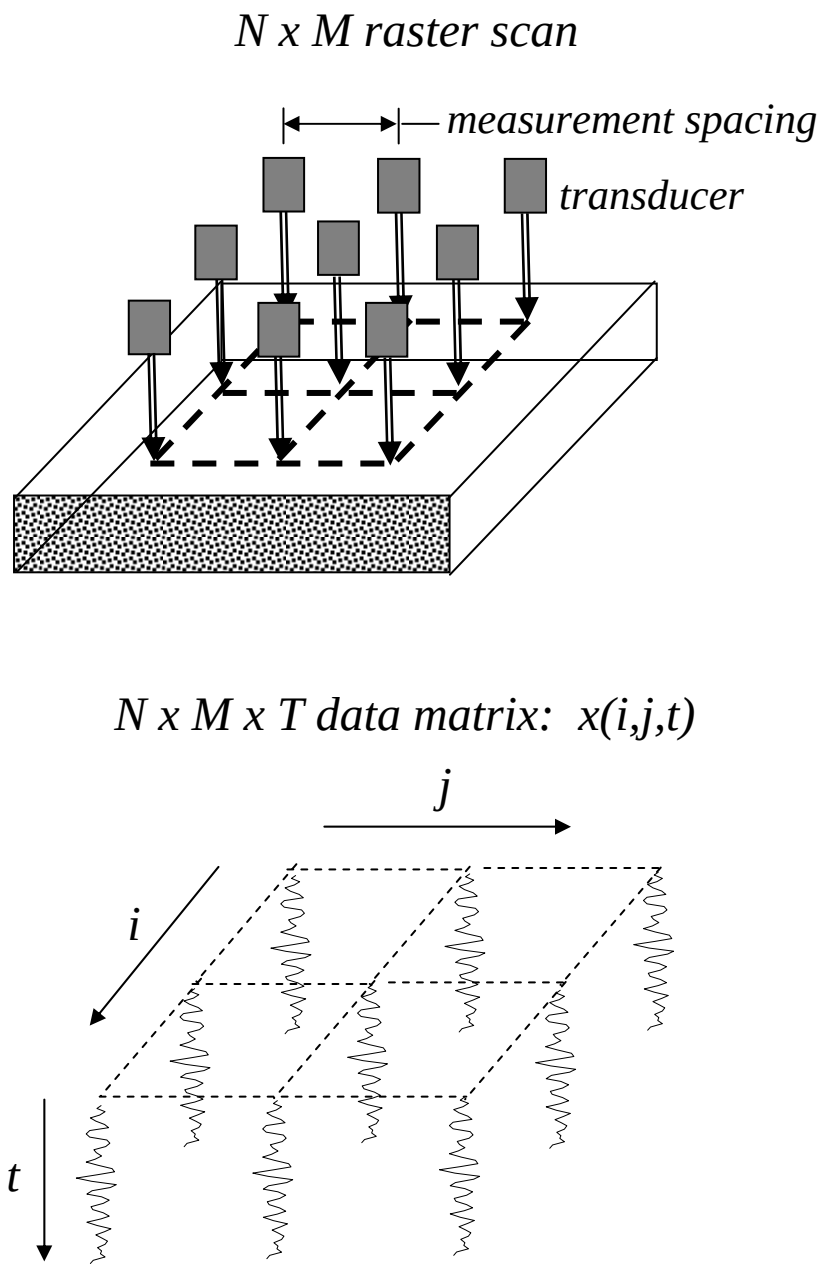

Figure 1. Schematic representation of a typical raster scan and data matrix.

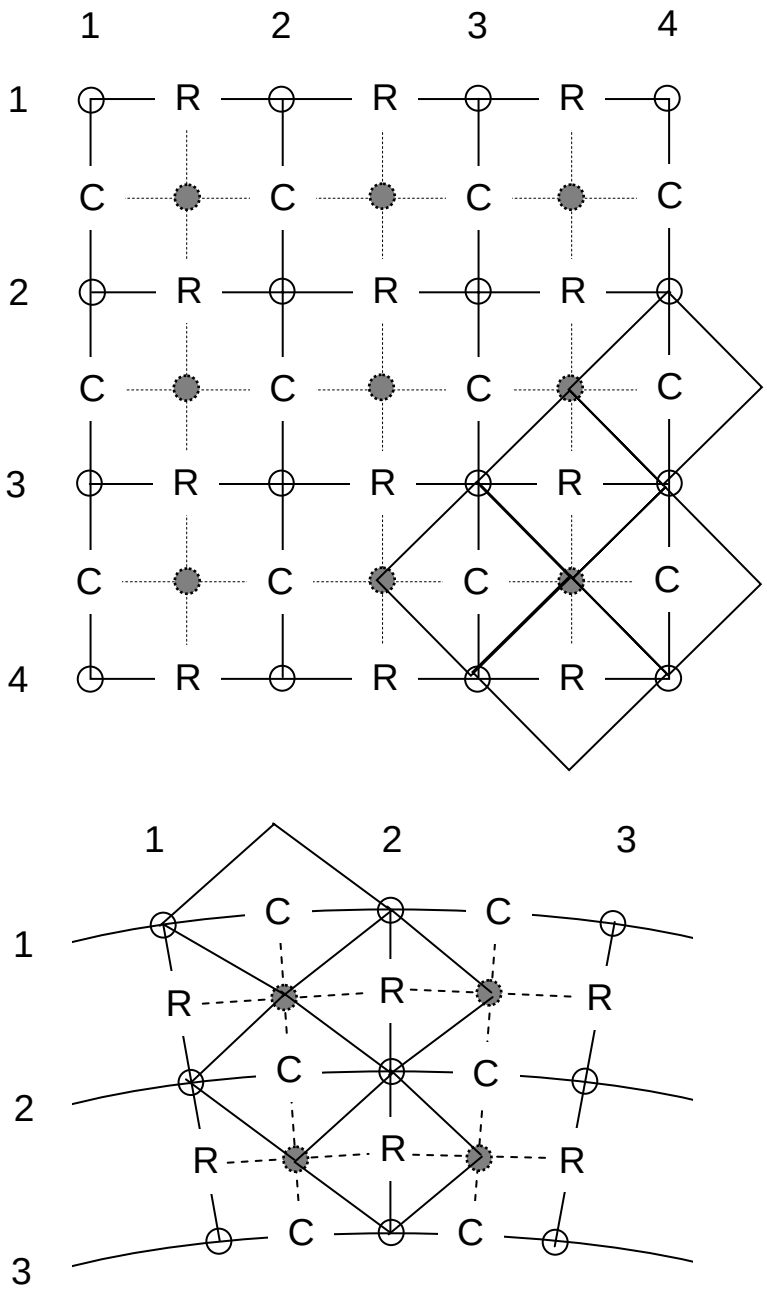

Figure 2. Schematic representation of Cartesian and polar scans. Open circles represent measurement positions. R's and C's represent the conceptual positions of row and column correlations for the Cartesian scan and radial and circumferential correlations for the polar scan.

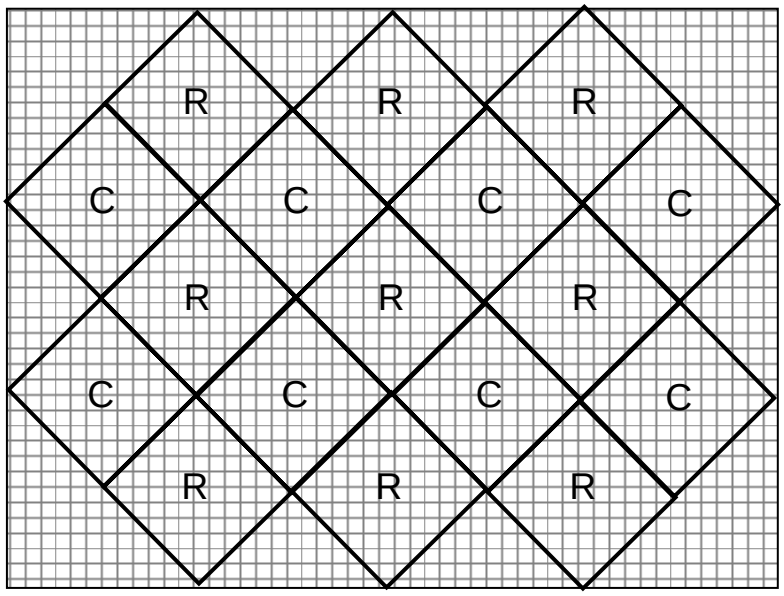

Figure 3. Correlation image display approach showing the highly discretized approach used to represent diamond regions surrounding row and column correlations.

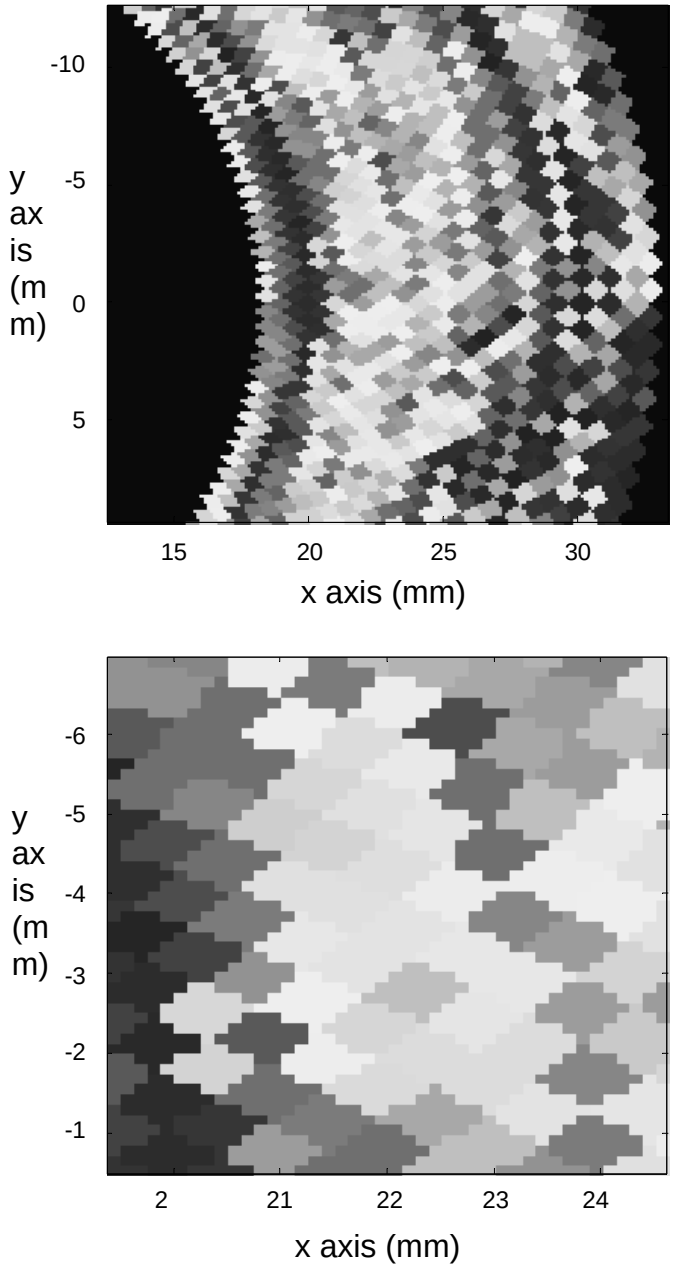

Figure 4. Example correlation images using the diamond region approach for a polar scan. Each diamond region represents either a radial or circumferential correlation coefficient. Images are shown at high magnification in order to reveal pixelization details.

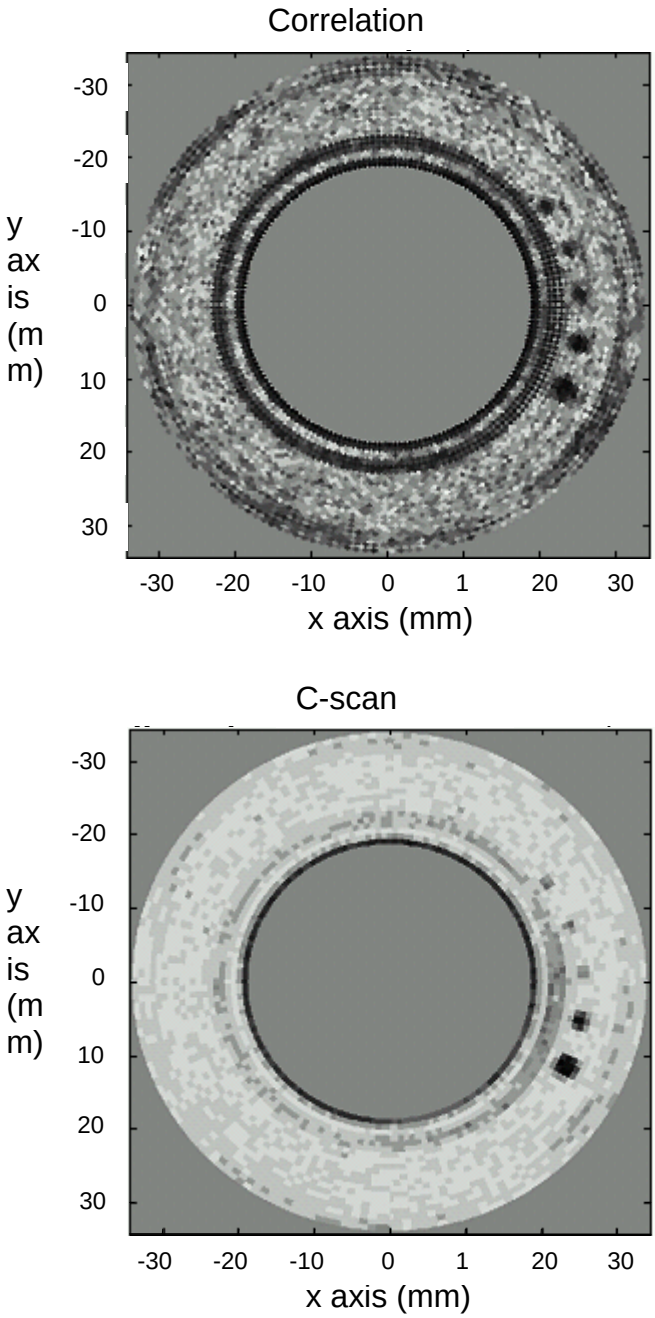

Figure 5. Example correlation image (top) and C-scan image (bottom) showing 5 flat bottom holes in a stainless steel annular ring. The correlation image was formed using the diamond region approach. The darker regions in the images represent high correlations or high amplitudes.

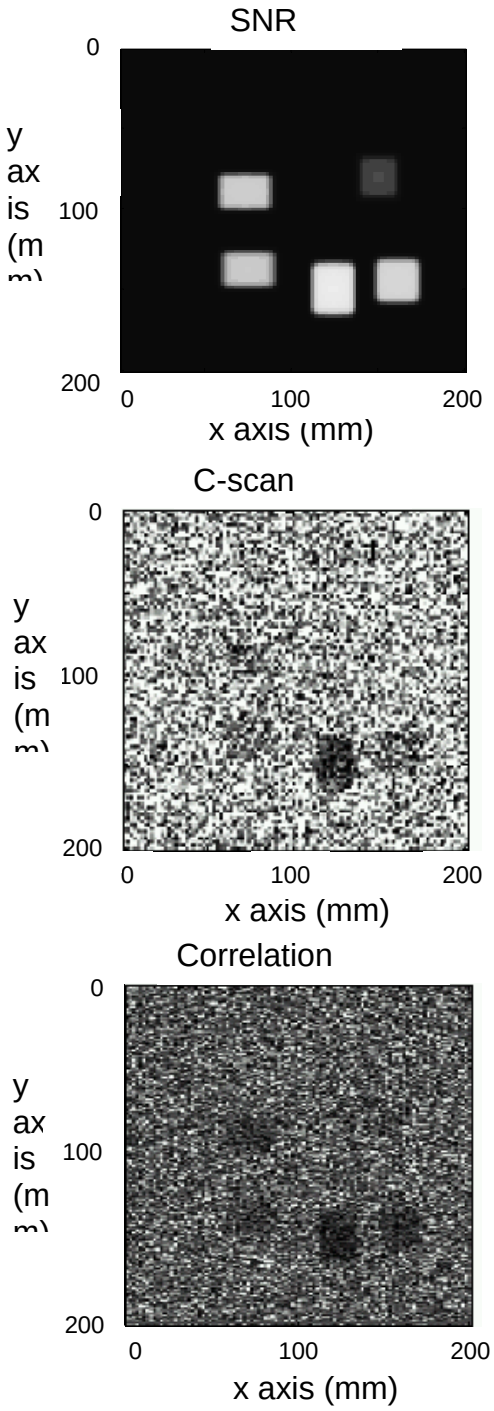

Figure 6. C-scan image (middle) and correlation image (bottom) showing detection of low SNR simulated defects in computer generated acoustic noise. The darker regions in the images represent high correlations or high amplitudes. The position and SNR of each defect is shown in the upper image. The correlation image was formed using the interleaving approach.

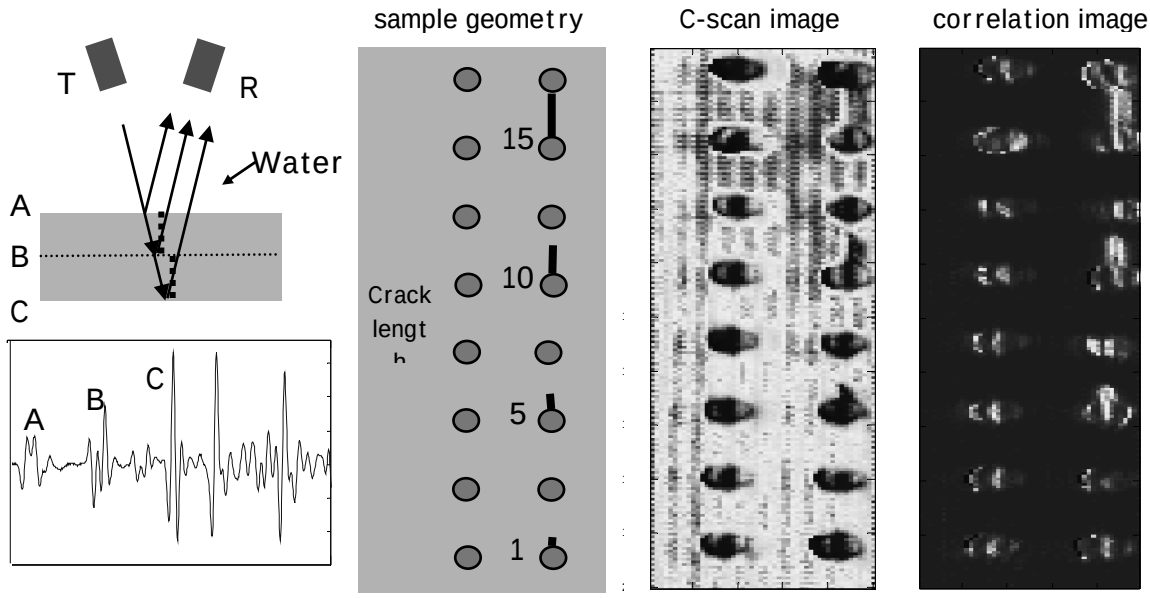

Figure 7. Example of crack detection in pitch-catch based on decreased correlations. Darker regions in the C-scan image represent decreased amplitude. Lighter regions in the correlation image represent decreased correlations. The correlation image was formed using the interleaving approach.